

Chemical-Grafting of Graphene Oxide Quantum Dots for Enhanced Electrochemical Analysis of Aromatics

Albina Mikhrallieva¹, Volodymyr Zaitsev^{1,2*}, Oleg Tkachenko^{3,4}, Michael Nazarkovsky¹ and Edilson V. Benvenuti⁴

¹ Department of Chemistry, Pontifical Catholic University of Rio de Janeiro, Marquês de São Vicente, 225, 22451-900, Rio de Janeiro, Brasil

² National University of Kyiv-Mohyla Academy, 2 Skovorody vul., Kyiv, Ukraine 04070

³ Materials Chemistry Department, V. N.Karazin Kharkiv National University, 4 Svoboda Square, Kharkiv, 61022, Ukraine

⁴ Institute of Chemistry, UFRGS, PO Box 15003, CEP, Porto Alegre, RS, 91501-970, Brazil

*E-mail: vnzaitsev@puc-rio.br

Abstract

Because of high surface area and combination of various functional groups, graphene oxide (GO) is currently one of the most actively studying materials for electroanalytical applications. Self-supported GO is not practical enough to be utilized individually and thus is commonly integrated with different supporting carriers. Having large lateral size GO can only wrap the particles of the support and thus, can significantly reduce the surface area of porous materials. To reach synergy from high surface area and polyfunctional nature of GO, and a rigid structure of porous support, the lateral size of GO must be essentially decreased. Recently reported graphene oxide quantum dots (GOQDs) can fulfill this task. We report successful preparation of mesoporous silica supported GOQDs exhibiting strong luminescent band with the maximum at 404 nm. From N₂ adsorption isotherms, it was demonstrated that the surface area of the resulted hybrid material was augmented. Raman spectrum of SiO₂-GOQDs shows two distinct peaks at 1585 cm⁻¹ (G-peak) and 1372 cm⁻¹ (D-peak) indicating presence ordered basal plane of graphene with aromatic sp² domains, and disordered oxygen-containing structure. Covalent immobilization of GOQDs on aminosilica via such oxygen-containing fragments was proved by FTIR, MAS ¹³C MNR, and XPS spectroscopy. SiO₂-GOQDs was used as a modifier of carbon paste electrode for differential pulse voltammetry determination of four environmental: sulfamethoxazole, trimethoprim, diethylstilbestrol (DES), and estriol (EST). The modified electrodes demonstrated an essential decrease in LOD for EST (220%) and DES (760%), which was explained by significant π - π stacking interaction between GOQDs and aromatic system of the analytes.

Keywords: graphene oxide quantum dots, immobilized nanoparticles, electroanalytical chemistry.

Introduction

Graphene oxide (GO) is one of the most commonly used carbon modifiers for preparation of various hybrid materials [1, 2]. Graphene oxide belongs to the class of 2D-nano objects (nanosheets) having up to several nanometers of thickness with the lateral size $>10^4$ nm. Macromolecule of GO has a huge surface area (up to $2630 \text{ m}^2 \text{ g}^{-1}$ [3]) and contains a basal plane of graphene with many oxygen-containing defects. Thus, it can interact with various molecules via non-covalent bonding including electrostatic, hydrogen and dative bonds, π - π stacking and dispersion forces [4, 5]. Because of its high surface area and polyfunctional nature GO has a great potential to be used for preconcentration of organic compounds containing aromatic rings and electronegative functional groups [6–9].

Self-supported 2D materials are not practical enough to be utilized individually. Due to strong π - π stacking and hydrophobic interaction between the graphene layers GO nanosheets can easily agglomerate and thus, drastically reduce their surface area. Therefore, GO is commonly integrated with different supporting carriers, such as mesoporous silica gels [10, 11], magnetic nanoparticles [12], carbon nanotubes, inorganic oxides, such as TiO_2 , Fe_2O_3 , MgO , etc., [13]. Since the lateral size of GO particles is about 10-100 μm which is 2-20 times bigger than in common silica particles, GO can only wrap silica particles (see, for example [10, 14]). If we take into account that at least 90% of the surface area of mesoporous silicas allocated in the pores, it becomes obvious that immobilization of flat non-porous nanosheet onto a surface of porous support instead of increasing, can significantly reduce the overall surface area of a hybrid material due to pore blocking. As a result, the adsorption capacity of SiO_2 @GO hybrid materials towards analytes can be much lower than individual GO and even SiO_2 . For example, SiO_2 @GO demonstrates ten times lower total adsorption capacity to Cu and Pb than silica-based adsorbent [14]. Unfortunately, in many recent publications, this effect was ignored that thus hybrid SiO_2 @GO materials have not shown their full potential [1, 15–17].

To reach synergy from high surface area and polyfunctional nature of GO, and a rigid structure of the porous support, the lateral size of GO must be essentially decreased. A lot of progress has been achieved in this direction, to tune properties of GO by downsizing its particles up to several nanometer scales [18–20]. New particles received by the downsizing of GO were signified to graphene oxide quantum dots (GOQDs) [21, 22]. Immobilized GOQDs demonstrate improved properties as adsorbents for HPLC [23], photonic/electronic devices [24], as carriers for photo-thermal and redox-responsive release of medications [25], as sensors in the electrochemical analysis [26]. In the latter case, smaller nanoparticles have better electrochemical properties [20].

Because of the miniaturization of electronics in recent years, the interest in electroanalytical methods has been growing, particularly in the rapid inexpensive determination of environmentally important contaminants in-field with portable instruments. The technical development associated with electrochemical sensors is an efficient, low-cost, fast-response and easy-to-operate alternative compared to spectroscopic or chromatographic ones. Besides, electrochemical devices have the advantage of portability and miniaturization [27]. Various materials have been used as working electrode in such devices: conductive

glasses [28], screen-printed [29], glassy carbon [30], ceramic carbon [31], and carbon paste [32]. To increase the electroactive area and facilitate the kinetics of the electrode/solution interface and thus sensitivity, the electrodes have commonly modified with metal/metal oxide nanoparticles [33, 34], carbon nanotubes [35], graphene [36] or GO [37], or with hybrid silica-based materials [38]. For example, it was found that the addition of mesoporous silica (SBA-15) to carbon paste electrode (CPE) can considerably enhance its sensitivity toward diethylstilbestrol [39], as much as immobilization of graphene on glassy carbon electrode [40]. Application of GOQDs as individual modifier as well as a part of hybrid material is under intensive electrochemical studies [29, 41]. For instance, the possibility of simultaneous determination of dopamine and epinephrine using gold nanocrystals capped with graphene quantum dots in a silica network was demonstrated recently [42].

Among biologically active compounds, which are inevitably discharged into the environment antibiotics and hormones require special attention. The residue of the antibiotics in the environment has resulted in bacterial resistance, which could seriously affect human health and ecological balance [43]. Environmental estrogens belong to a group of endocrine disruptors (ED) and can cause cancerous tumors, birth defects, and other developmental disorders of the endocrine system even at low concentrations [44–46]. Hence, it is important to develop analytical methods for time- and cost-effective monitoring of ED in various media. It seems that electrochemical sensors can resolve this demand [47].

The idea of the current research was to integrate supporting and size-selective properties of mesoporous silica network, and electroactive properties of GOQD in order to obtain high surface area working electrode with an enhanced affinity towards chemicals having aromatic or heterocycle fragments. As model compounds, we selected next endocrine disruptors: sulfamethoxazole (SMZ) and trimethoprim (TMP) (antibiotics), diethylstilbestrol (DES) and estriol (EST) (hormones). Selected medications have various polar functional groups as well as aromatic and heterocyclic fragments, allowing their multiple-point interaction with GOQDs surface, Fig. 1.

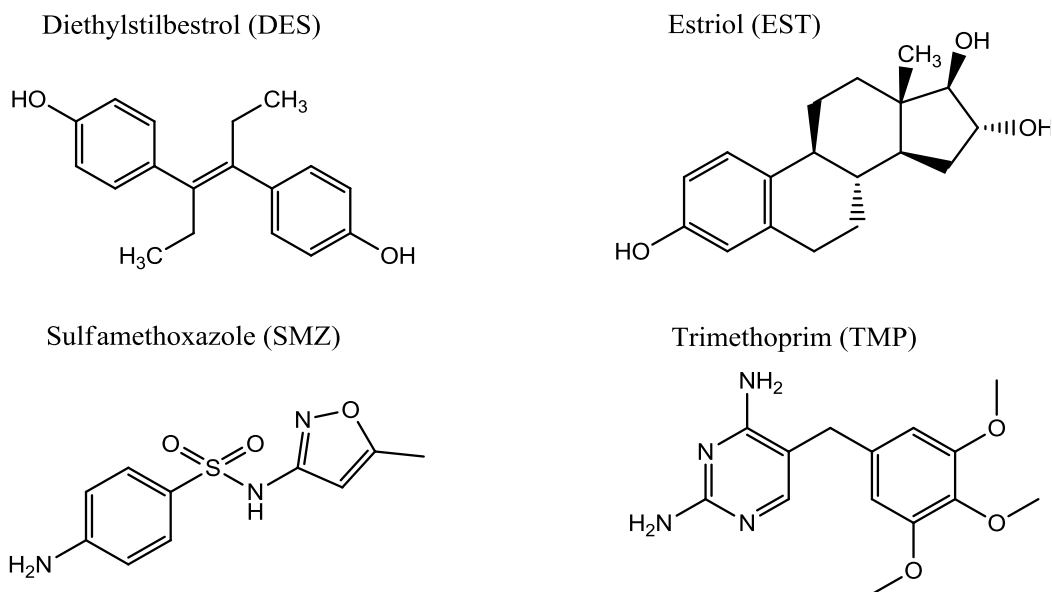


Fig. 1 Chemical formulas of medications studied in this research

This interaction can increase the sensitivity of the electrode towards analytes and improve the selectivity of the analysis. With this aim in view, hybrid SiO₂-GOQDs material was prepared and characterized by MAS NMR ¹³C, XPS, Raman and FTIR spectroscopies, electron microscopy (SEM) and solid-phase photoluminescence spectroscopy. To prevent possible side-reactions on electrocatalytically active Mn-sites [48–50] special attention was given on the preparation of Mn-free GOQD.

Materials and methods

Chemicals and reagents

Silica gel with 4 nm average pore size and 63-200 μm particle size distribution was purchased from Merck, (3-Aminopropyl)triethoxysilane (APTES, ≥98%), toluene anhydrous, N,N'-dicyclohexylcarbodiimide (DCC, 99%), potassium permanganate (KMnO₄, ≥99.0%), hydrogen peroxide solution (H₂O₂, 30 % (w/w)) were purchased from Sigma–Aldrich. Ninhydrin (99%) and sulfuric acid (95-98%) were provided by QHEMIS (Brazil), graphite and dimethylformamide (99.8%) – from Synth (Brazil). Diethylstilbestrol, estriol (both 97%), sulfamethoxazole (SMZ, 98%) and trimethoprim (TMP, 98%) were from Sigma-Aldrich. Britton-Robinson buffer (0.04 mol L⁻¹) was prepared from the following reagents: boric acid (Neon, 99.5%), acetic acid (Dinamica, 99.7%), phosphoric acid (Vetec, 85%), hydrochloric acid (Merck, 37%), sodium hydroxide (Vetec, 97%), sodium nitrate (Quimica Moderna, >99%). After distillation with calcium hydride (Sigma-Aldrich), toluene was kept in a dark bottle with 3 Å molecular sieves (4-8 mesh, Sigma-Aldrich). The aqueous solutions were prepared using ultra-pure water from PURELAB Classic, Elga, UK).

Characterization techniques

The solution pH was measured using a PHS-3E pH-meter with BioTrode (Hamilton, USA) ion-selective electrode. The electrical conductivities of suspensions were measured using HI 8633 conductivity meter (HANNA instruments, UK). The concentrations of manganese ions in solutions were determined by Optima 7300 DV Inductively Coupled Plasma Optical Emission Spectrometry (Perkin Elmer), and in ZEE nit 60 Atomic Absorption Spectrometer with a transversely-heated graphite furnace (Analytik Jena AG, Germany). The specific surface area and pore size of silica gels were determined from nitrogen adsorption/desorption isotherms on Tristar II 3020 Kr (Micromeritics, USA). Elemental analysis (CHN) of the samples was done on PE-2400 elemental analyzer (Perkin Elmer, USA) and loading of immobilized groups was calculated from Eq.1.

$$C_L(\text{mmol g}^{-1}) = \frac{10 \cdot P_e}{A_r \cdot n_e}, \quad \text{Eq.1}$$

where P_e is the content of element, %; A_r is the element atomic mass; n_e is the number of atoms of the element in the grafted fragment.

Fourier transform infrared spectroscopy (FTIR) spectra were recorded in the region 4000-400 cm^{-1} on FTLA-2000 spectrometer (Thermo Scientific Nicolet). Solid-state ^{13}C and ^{29}Si CP/MAS NMR of the samples were obtained on Agilent Technologies DD2 500/54A (Agilent, USA) - 100.6 MHz (^{13}C). UV-Vis absorption spectra were measured on a Cary 100 (Agilent, USA). The composition of hybrid materials was determined from X-ray photoelectron spectroscopy (XPS), using a K-Alpha X-ray photoelectron spectrometer (Thermo Fisher Scientific, UK) equipped with a hemispherical electron analyzer and an aluminum anode X-ray source ($K\alpha = 1486.6$ eV) at the energy resolution of ~ 1 eV. For organic analytes, octane-water distribution coefficients (P) were calculated using software ChemDraw Ultra 12.

The concentration of immobilized functional groups (CL) was calculated from Eq. 2.

$$C_L(\text{mmol g}^{-1}) = \frac{1000 \cdot at(N)}{at(Si) \cdot M(\text{SiO}_2)} \quad \text{Eq. 2}$$

where $at(Si)$ and $at(N)$ are the atomic percentage of Si and N in the hybrid, respectively; $M(\text{SiO}_2)$ is SiO_2 molar mass.

The morphology of the samples was studied on a low-vacuum JSM-6490LV scanning electron microscope (SEM) (JEOL, Japan). Differential pulse voltammograms (DPVs) were recorded on IviumStat potentiostat/galvanostat (Ivium Technologies, The Netherlands) with a conventional three-electrode cell. Modified carbon paste electrode (CPE, working electrode), platinum wire (the auxiliary electrode) and Ag/AgCl (reference electrode) were mounted in the cell. For DPV the following parameters were used: pulse amplitude of 50 mV, pulse time of 50 ms, step potential of 1 mV and scan rate of 10 mV s^{-1} . From each voltammogram the background was subtracted, as commonly recommended [51]. The limit of

detection (LOD) and limit of quantification (LOQ) were calculated as next: $LOD = 3S_b/b$, and $LOQ = 10S_b/b$ where S_b is the standard deviation of the blank ($n = 10$) and b is the slope of the calibration curve.

Synthesis of graphene oxide quantum dots

GOQDs were prepared in one-step ultrasonic synthesis [52]. In brief, 200 mL of a mixture of concentrated H_2SO_4 and H_3PO_4 (9:1 v/v) was added to graphite powder (1.5 g) in a 500-mL round-bottom flask equipped with a mechanical stir bar. Then $KMnO_4$ (9 g) was added slowly at room temperature under stirring and after the flask was heated to 50 °C and kept at this temperature for 12 h. The obtained lite-pink mixture (Fig. S1a) was cooled down, poured slowly onto ice (400 mL) with 30% H_2O_2 (20 mL) giving orange suspension, Fig S1b. The solid was separated by centrifugation and washed with water. To remove manganese impurities, the precipitate was immersed into HCl (2%) then separated from the solution by centrifugation. The procedure was repeated until negative results on Mn in solution with ICP-OES. Finally, 40 mg of freeze-dried film (Fig S1d) was sonicated in 50 mL of DMF for about 2 h. Emitting green-blue light in UV irradiation dispersion was subjected to further immobilization.

Preparation of SiO₂-GOQDs hybrid material

GOQDs were covalently immobilized on silica gel surface via silica-immobilized aminosilane and carboxylic groups of GOQDs, as described elsewhere [7]. Typically, activated in HNO_3 and dried at 500 °C silica gel (10 g) was suspended in 100 mL of dry toluene and 3 mL of APTES was added under constant stirring. The reaction mixture was refluxed for 10 h, filtrated, washed in a Soxhlet apparatus with toluene for 24 h and finally dried in vacuum at 120 °C for 7 h. The resulted aminosilica (SiO_2-NH_2), (3 g) was added to the suspension of GOQDs in 50 mL of DMF and 40 mg of DCC were added under stirring. The suspension was heated at 85 °C for 60 h with periodic sonification for 30 min. Solid-phase was separated by decantation, washed with DMF, methanol and water under ultrasonic treatment (5 min). Finally, the precipitate was dried at 120 °C for 8 h to obtain about 3 g of SiO_2 -GOQDs. Chemical analysis of SiO_2-NH_2 and SiO_2 -GOQDs revealed augmented carbon content in the samples - from 2.89 to 3.22% (Table S1), while the percentage of nitrogen did not change. This indicated that about 3.3 mg of GOQDs has been immobilized per one gram of SiO_2 -GOQDs, which constitute 25% from initially loaded for synthesis (13 mg/g).

Preparation of CPE modified electrode

Typically, 8 mg of SiO_2 -GOQDs and 12 mg of graphite powder were carefully mixed in an agate mortar with addition of mineral oil (5 mg). The prepared homogeneous paste was placed in a Teflon cavity (1 mm in depth and 2 mm in diameter), covered with a platinum disk fused to a glass tube with copper wire as an electric conductor. The manufactured electrode was denoted as CPE/Si/GOQD. Unmodified CPE electrode, fabricated in the same way without SiO_2 -GOQDs was used for the comparative analyses.

Results and discussion

Synthesis approach

Hybrid SiO₂-GOQDs materials can be obtained by adsorption and further chemical anchoring of the preliminarily prepared GOQDs on the support surface [4, 25, 53]. As an alternative way is incomplete pyrolysis of small organic compounds trapped inside of the adsorbed pores [54]. In the latter case, porous matrix can better confine the size and shape of the resulted GOQDs [55, 56]. However, preparation of SiO₂-GOQDs inside the host porous system can have an undesirable effect, since it can, as mentioned above, essentially reduce the specific surface area of the resulted hybrid material. For example, SBA15-GQDs nanocomposite prepared by incomplete pyrolysis of pyrene adsorbed in SBA15 pores has only 26 m² g⁻¹ while the specific surface area of the pristine host was 719 m² g⁻¹ [55]. Therefore, the first scheme has been selected and GOQDs were prepared from graphite in one-step ultrasonic synthesis with further immobilization of appropriate nanoparticles in the porous system of mesoporous silica. The ability of GOQDs to infiltrate into silica pores have been confirmed recently [26, 57]. Samples of GO were prepared from graphite powder by oxidation with KMnO₄ in the mixture of concentrated H₂SO₄ and H₃PO₄, because it was demonstrated that the introduction of H₃PO₄ to the acid mixture improved safety of the process and led to the successful increase in the reaction yield [58].

It was important to obtain metal-free nanocomposite [55] since even traces of electrocatalytically active metal ions such as Mn can corrupt properties of SiO₂-GOQDs electrodes [48, 59, 60]. To ensure Mn-free composition of GO samples, the concentration of Mn ions in washing solutions was monitored. The results presented in Fig. S2 demonstrates that for removal of Mn²⁺ ions impurities from GO by water are less sufficient than washing with 2% HCl. This fact can be explained by good adsorption properties of GO towards metal ions [1, 61].

Covalent immobilization of GOQDs on silica surface was performed via well-established procedure of SiO₂-NH₂ acylation in anhydrous solvent (DMF) by carboxylic functional groups of GOQDs in the presence of DCC [10, 14]. Excess of GOQDs was separated from the final product by multiple decantations of the precipitate alternating with the ultrasonic treatment of SiO₂-GOQDs in DMF. Finally obtained grey product demonstrates greenish luminescence under irradiation with UV light at 365 nm, Fig. 1d.

Characterization of SiO₂-GOQDs

Nitrogen adsorption/desorption measurements

From Fig. 2, it can be seen that samples SiO₂-GOQDs have the identical character of N₂ adsorption/desorption isotherm that pristine SiO₂-NH₂. This suggests that immobilization of GOQDs does not change the porous structure of silica support having typical Type IV isotherm with a distinct hysteresis loop of H1 within the p/p₀ range of 0.4–1.0, indicating mesopore presence. At high relative pressure, the saturation of the isotherms is clearly observed and this feature indicates the complete filling of the

mesopores and the absence of macropores. The very similar isotherm profile and surface area values evidence that the addition of GOQDs does not produce significant textural changes. However, from slightly higher average pore volume and pore size for SiO₂-NH₂ and larger surface area for SiO₂-GOQDs (Table 1) incorporation of GOQDs to the porous structure of hybrid material can be assumed.

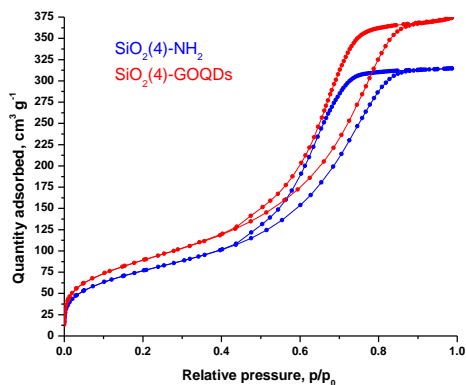


Fig. 2 N₂ adsorption/desorption isotherms of SiO₂-NH₂ (blue curve) and SiO₂-GOQDs (red curve)

The maintenance of the textural properties is an excellent result regarding that the material will be applied as an electrochemical sensor. The presence of graphene domains provides electrical conductance and at the same time, the material maintains the porosity that allows the diffusion of the electroactive species and provides high electroactive area [38].

The BET surface area of modified material increases by about 15%. This increase was interpreted considering a contribution from the graphene oxide that presents high surface area. This contribution can be seen from the profile of the isotherms. After the graphene oxide addition, an increase in the amount of adsorbed nitrogen occurs, even in low relative pressures ($P/P_0 < 0.2$), which is related to the micropores, probably contribution of the graphene sheets [3].

Table 1. The textural characteristics of the obtained materials.

Material	Average pore size, nm	S _{BET} , m ² g ⁻¹
SiO ₂ -NH ₂	5.4	278
SiO ₂ -GOQDs	5.2	324

SEM

The morphology of GO and SiO₂-GOQDs was investigated by SEM technique. Freeze-dried GO demonstrates a closely packed lamellar texture reflecting its multilayered microstructure, (Fig. 3a inset). With the exfoliation of graphite oxide into GO, the edges of the GO sheets become crumpled, folded, and

closely restacked. The GO sheet has a rough surface of the film (Fig. 3a). SEM image of SiO₂-GOQDs obviously demonstrates that silica particles have not wrapped by GO and thus porous structure of the hybrid SiO₂-GOQDs composite is open. It is in agreement with the conclusions made from N₂-adsorption isotherms above.

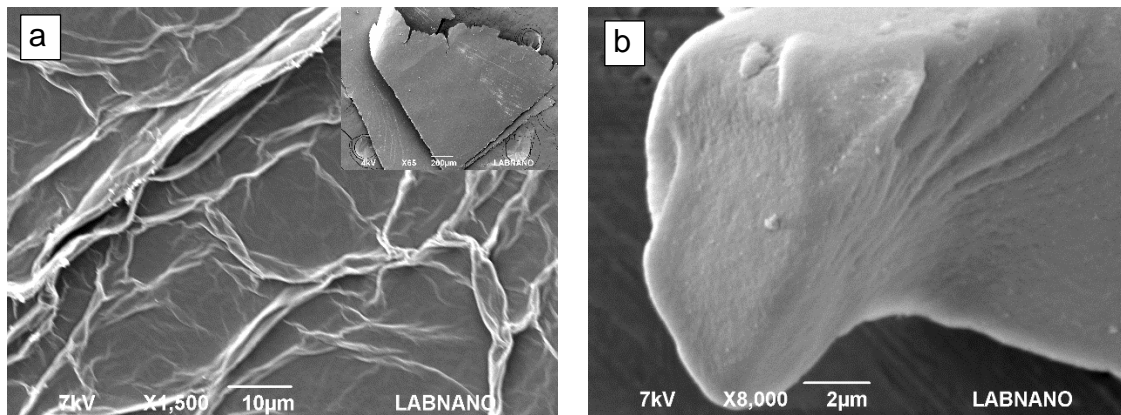


Fig. 3 SEM images of GO(a) and SiO₂-GOQDs (b)

Fluorescence spectroscopy

Photoluminescent spectra of SiO₂-GOQDs serve as positive proof of GOQDs immobilization on SiO₂ surface. It is known that neither aminosilica, nor GO exhibit photoluminescence, but SiO₂-GOQDs exhibit strong luminescent band with the maximum at 404 nm (Fig. 4), likewise GOQDs in water suspension [24] and other hybrid silica-based materials with loaded GOQDs [21, 26].

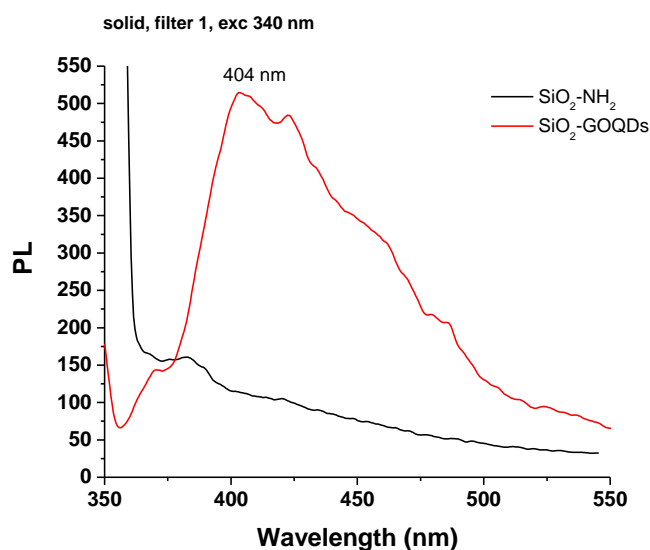


Fig. 4 Photoluminescent spectra of solid SiO₂-NH₂ (—) and SiO₂-GOQDs (—) under excitation at 340 nm.

Raman spectroscopy

To investigate the successful synthesis of GOQDs and immobilization of the nanoparticles obtained on silica surface, the Raman spectra of GOQDs and SiO₂-GOQDs were recorded. From Fig. 5 it is evident that the Raman spectrum for GOQDs shows two distinct peaks at 1585 cm⁻¹ (G-peak) and 1372 cm⁻¹ (D-peak).

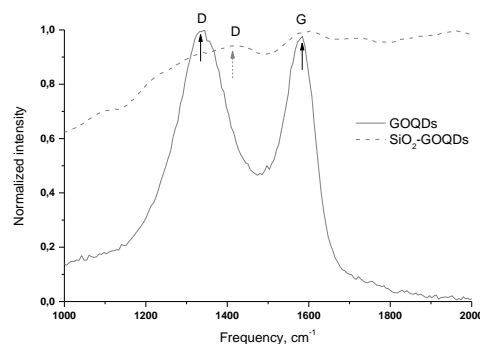


Fig. 5 Raman spectra of GOQDs (—) and SiO₂-GOQDs (- -).

The D peak is an indication of the disordered structure of graphene in GOQDs due to oxidation. The G peak from the ordered basal plane of graphene is observed at 1585 cm⁻¹. The ratio between the intensities of characteristic bands (I_D/I_G) gives an indication of the functional group insertion [62]. For experimental samples $I_D/I_G < 1$ presumably indicating a decrease in the fraction of aromatic sp² domains in GOQDs with increasing the number of detection oxygen-containing sites [63]. Further similar evidence for oxygen-containing groups in GOQDs was received from FTIR, NMR MAS and XPS of the SiO₂-GOQDs hybrid material. Despite strong fluorescence background and low carbon content, we were able to record Raman spectrum from SiO₂-GOQDs and it confirms immobilization of GOQDs, Fig. 5. Ordered G band was detected at about 1585 cm⁻¹ that matches the position of G band of individual GOQDs indicating negligible interaction between silica scaffold and basal plane of immobilized GOQDs. Contrary, the position of D-band in hybrid material is shifted to 1412 cm⁻¹ Fig. 5, suggesting anchoring of GOQDs via oxygen-containing sites. It is obvious that not all such sites of GOQDs react with immobilized aminosilane fragments in SiO₂-NH₂. Therefore D-band in Raman spectra of SiO₂-GOQDs is proliferated, Fig. 5.

FTIR characterization

The FTIR spectra of SiO₂-GOQDs, as well as Raman spectra, suggest the presence of oxygen-containing sites in GOQDs, including C(O)O-H (ν_{O-H} at 3390 cm⁻¹), CO-H (ν_{O-H} at 3250 cm⁻¹) and carboxyl ($\nu_{C=O}$ at 1730 cm⁻¹) moieties [6], Fig. 6.

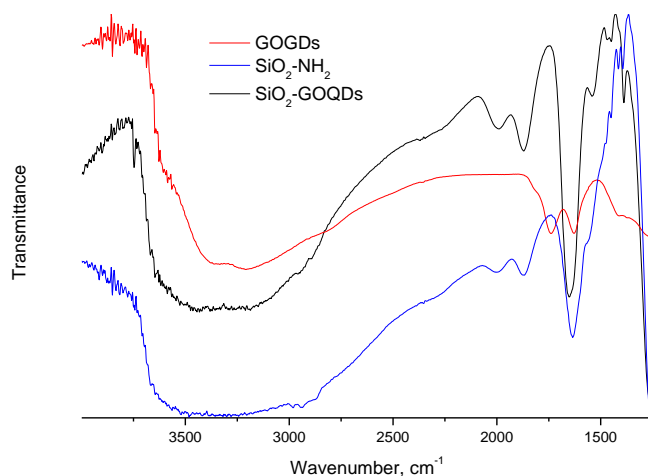


Fig. 6 FTIR spectra of GOQDs, SiO₂-NH₂, SiO₂-GOQDs

Apart of silica gel matrix, the pristine SiO₂-NH₂ shows several bands at about 2950 cm⁻¹ (ν_{CH_3} and ν_{CH_2}), and at peaks at 1560, 1475, 1450 1420 and 1390 cm⁻¹ that correspond to stretching vibrations of propylamine chain. FTIR spectrum of GOQDs essentially changed on immobilization. Particularly, stretching vibration of the carboxylic group at 1730 cm⁻¹ disappeared, and bands at 1650 cm⁻¹ and 1574 cm⁻¹ corresponding to stretching vibration of C=O and bending vibrations of N-H in NHC(O) fragment of immobilized moiety developed instead, Fig. 6. From these observations, covalent immobilization of GOQDs via carboxyl fragments of the nanoparticle and aminogroup of the silane can be assumed [6, 23].

MAS ¹³C NMR spectroscopy of SiO₂-GOQDs.

The SiO₂-GOQDs have low (less than four percent) total carbon content, therefore ¹³C MAS NMR spectrum of this nanocomposite is very noisy, Fig. 7.

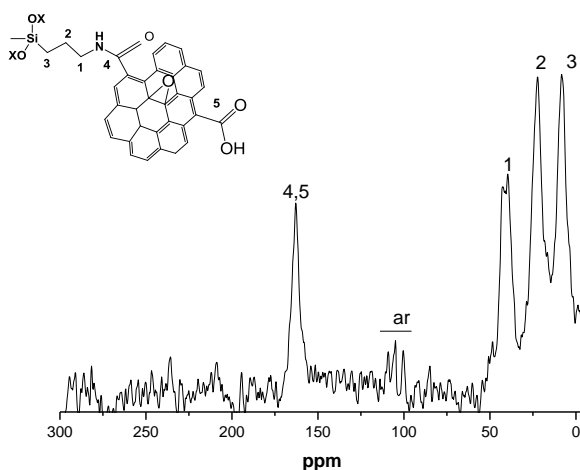


Fig. 7 CP/MAS ^{13}C NMR spectrum of SiO_2 -GOQDs

Nevertheless, we were able to record the spectra and identify the signals. Intensive peaks at 10, 25, and 40 ppm were correspondingly assigned to $\text{Si-C}_\alpha\text{H}_2$, $\text{CH}_2\text{-C}_\beta\text{H}_2$ and $\text{C}_\gamma\text{H}_2\text{-NH-}$ in immobilized moiety, Fig. 7. A signal at 165 ppm was identified as carbonyl fragment of GOQDs [64, 65], while series of signals at 100-115 ppm were assigned to sp^2 carbons in the basal plane of graphene [66]. Consequently, ^{13}C NMR spectrum of SiO_2 -GOQDs as well as FTIR and Raman demonstrate an essential fraction of oxygen-containing fragments in GOQDs and prove immobilization of the GOQDs in the porous scaffold of silica.

XPS spectroscopy

XPS spectra of SiO_2 -GOQDs further confirmed the successful immobilization of nanoparticles. As demonstrated, SiO_2 -GOQDs is Mn-free material, since its XPS does not contain Mn 2p peaks at 641.3 and 653.2 eV [67], Fig. 8a.

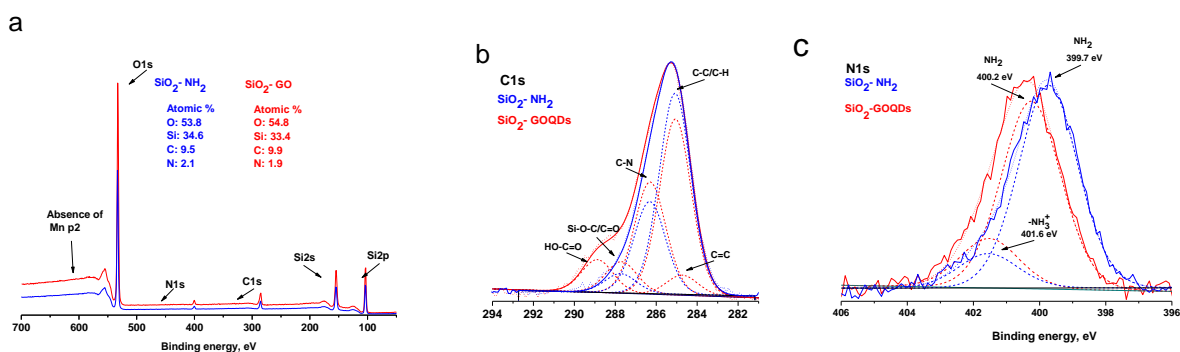


Fig. 8 Survey (a) and fitted XPS spectra of the C1s (b) and N1s (c) of SiO_2 -GOQDs and pristine $\text{SiO}_2\text{-NH}_2$ with deconvoluted data (d) regions corresponding to $\text{SiO}_2\text{-NH}_2$ and SiO_2 -GOQDs.

The high-resolution XPS spectra demonstrate the essential difference between C1s bands for $\text{SiO}_2\text{-NH}_2$ and SiO_2 -GOQDs, Fig. 8b. The C1s band from $\text{SiO}_2\text{-NH}_2$ can be deconvoluted into three components attributed to C-C, C-N and C-O bonds in SiO_2 -immobilized aminopropyl fragments, Table 2. The relative intensity of C-C and C-N peaks in the spectrum is about 3:1, which correlates with the composition of the immobilized fragment. Also, about 6% of carbon atoms in $\text{SiO}_2\text{-NH}_2$ bonded with oxygen, which lets us assume the occurrence of incomplete hydrolysis of ethoxy groups of aminosilane in the immobilization process, as it is demonstrated in Fig. 7(inset). The high-resolution XPS C1s spectra of SiO_2 -GOQDs among the signals from $\text{SiO}_2\text{-NH}_2$ shows additional peaks (Fig. 8b), attributed to C=C and C=O bonds in O-C=O or N-C=O fragments (Table 2), indicating successful immobilization of GOQDs [14].

Table 2. XPS analysis of SiO_2 -GOQDs and pristine $\text{SiO}_2\text{-NH}_2$

$\text{SiO}_2\text{-NH}_2$	$\text{SiO}_2\text{-GOQDs}$
C1s	

Type	C-H, C-C	C-N	C-O	C=C	CH, C-C	C-N	C-O	OCO
eV	285.1	286.3	287.7	284.7	285.1	286.2	287.7	288.9
%	69	25	6	5	47	31	8	9
N1S								
	NH ₂	NH ₃ ⁺	NH		NH ₃ ⁺			
eV	399.7	401.6	400.2		401.6			
%	86	14	79		21			
C _L = 1.01 mmol g ⁻¹				C _L = 0.95 mmol g ⁻¹				

Fig. 8c illustrates the high-resolution N1s XPS spectra of the synthesized hybrids. Band of pristine SiO₂-NH₂ consists of components attributed to neutral and protonated primary amines. On GOQDs immobilization fraction of H-bonded amines noticeably increased, while another fraction of amine fragments was transformed to amide, Table 2. This effect reflects a peculiarity of the surface reaction of the immobilized amine with nanoparticles containing several carboxyl fragments. It should be readily apparent that only few carboxyl groups of GOQDs can acylate immobilized amines due to steric restrictions. Others will be ionized and will protonate the remaining amines, as it is illustrated in Fig. 9.

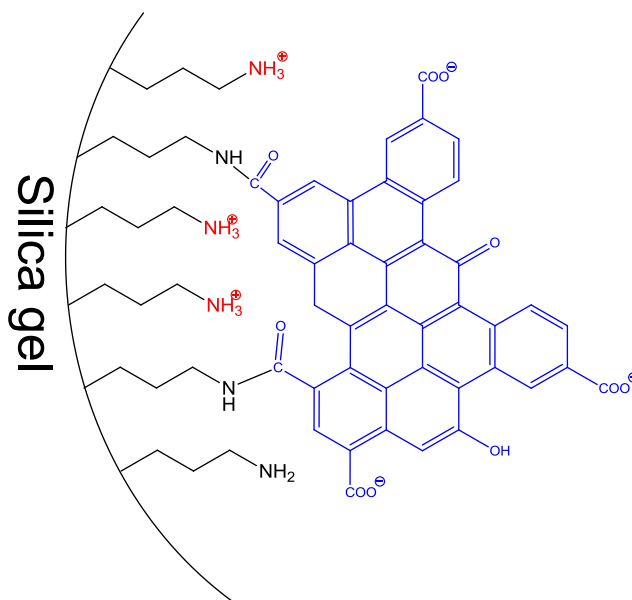


Fig. 9 Schematic structure of surface layer in SiO₂-GOQDs

Electrochemical properties of the carbon paste electrode modified with SiO₂-GOQDs

Carbon paste electrode (CPE) was selected for modification because it is cheap, can be reproducibly fabricated in any laboratory and SiO₂-GOQDs can be easily integrated into the electrode. Two

antibiotics and two hormones were selected for investigation, namely: sulfamethoxazole and trimethoprim, diethylstilbestrol and estrogen estriol, Fig. 1. Diethylstilbestrol is the first synthetic estrogen that had been extensively used in the treatment of estrogen-deficiency disorders. Nowadays, DES is often illegally used as growth-promoter for cattle, sheep and poultry in many countries [68]. Although it had been prohibited as a growth promoter for years, these estrogens are still found in the river [69], fish [70], milk [71], and meat [8].

All selected analytes have aromatic rings that can form π - π stacking complexes with GOQDs, but they also have various polar fragments, with can weaken or enhance such interaction and thus change the sensitivity of the electrochemical analysis. First, the CPE electrode modified with SiO₂-GOQDs was tested in differential pulse voltammetry (DVP) oxidation of a mixture, containing sulfamethoxazole and trimethoprim (5:1). The results were compared with those, obtained on the CPE electrode without any additives.

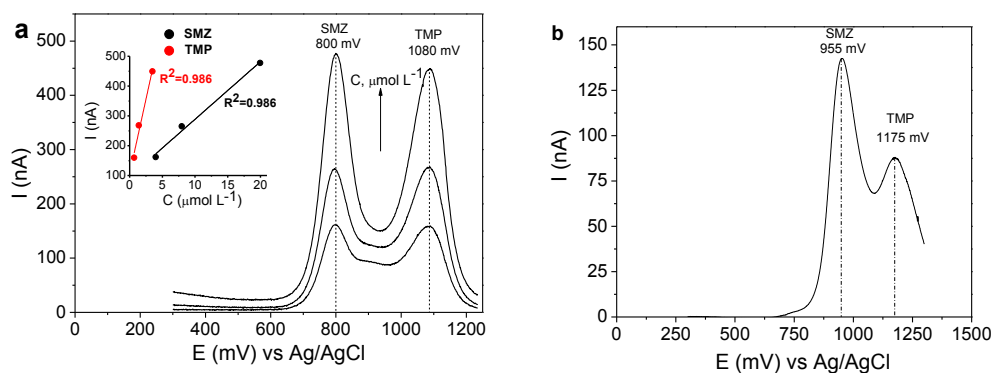


Fig. 10. DPV analysis of sulfamethoxazole (SMZ) and trimethoprim (TMP) on modified with SiO₂-GOQDs (a) and bulk (b) carbon paste electrodes. The analytes were present in a mixture (5:1) with the next concentration of SMZ: a) 4.0, 8.0 and 20 $\mu\text{mol L}^{-1}$; b) 4.0 $\mu\text{mol L}^{-1}$. Supporting electrolyte: 0.04 mol L^{-1} of BRbs (pH 5.8), 0.5 mol L^{-1} of NaNO₃.

From the data presented in Fig. 10 it is amply clear that electrode modified with SiO₂-GOQDs has higher response to TMP (87% of enhancement) and only 14% to SMZ. Further, the oxidation peaks are shifted to lower potentials for both components but differently (-155 mV for SMZ and -95 mV for TMP). This effect contributes to the difference in anodic peaks of analytes to 280 mV making determination of SMZ and TMP in their simultaneous presence more reliable. Improved sensitivity and better-separated peaks point to a benefit of SiO₂-GOQDs on electrochemical analysis of SMZ and TMP by DVP.

The significant improvement of the electrocatalytic performance of the modified electrode was also observed in the DVP analysis of both selected hormones. In DES analysis the modified electrode demonstrated 7.6-fold enhancement of sensibility and by 2.2-fold in EST analysis compared to the bare electrode, Fig. 11. Similarly, to the results of the antibiotics analysis, the oxidation peaks of both hormones

are shifted to lower potentials for SiO₂-GOQDs modified electrode in comparison with the neat one, attesting better interaction of the analytes with active centers of the electrode.

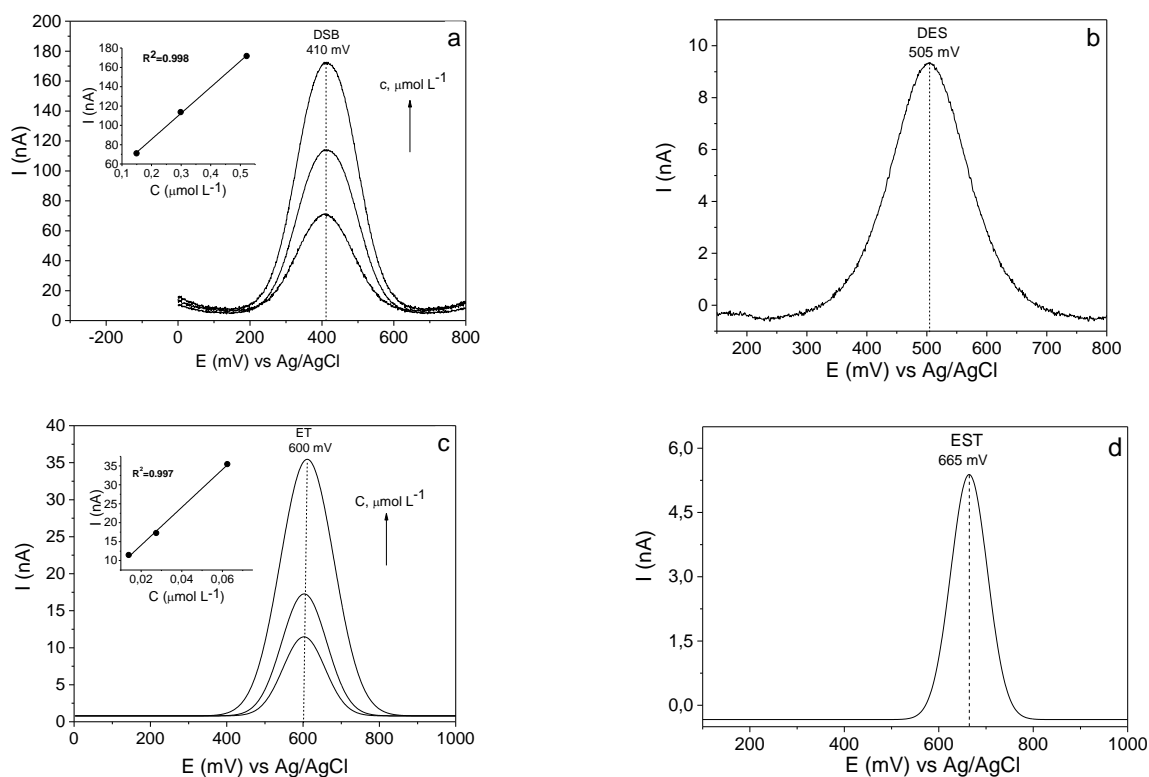


Fig. 11 DPV analysis of DES (a,b) and EST (c,d) on modified with SiO₂-GOQDs (a,c) and bulk (b,d) carbon paste electrodes. Concentration of the analytes: DES - 0.15, 0.30 and 0.52 $\mu\text{mol L}^{-1}$, EST - 0.014, 0.027, 0.062 $\mu\text{mol L}^{-1}$. Supporting electrolyte: 0.04 mol L⁻¹ of BRbs (pH 5.8), 0.5 mol L⁻¹ of NaNO₃.

The modified electrodes demonstrated linear signal response vs. concentration of the analytes according to the equations that are presented in Table S2 along with LOD and LOQ for the current modified electrode and other electrodes reported earlier. From the data presented it can be seen that CPE modified with SiO₂-GOQDs evinces the lowest value of LOD for EST and DES. These results can be explained considering the textural characteristics and chemical nature of SiO₂-GOQDs. As demonstrated earlier, the integrated of mesoporous silica to graphite paste electrode can enhance its electrochemical response due to the enlargement of the electroactive sites on the electrode surface [38]. Immobilization of GOQDs improves the affinity of the resulted modified electrode to the analytes that can interact with immobilized electroactive fragments, such as basal aromatic domains in GOQDs. Indeed, from the analysis of the results presented in the Table S2, electrode modified with SiO₂-GOQDs has much higher sensitivity towards more lipophilic EST (500 nA L μmol^{-1}) and DES (270 nA L μmol^{-1}) then to SMZ (19 nA L μmol^{-1}) and TMP (100 nA L μmol^{-1}), which are more polar (Fig. S3). But only higher lipophilicity of the hormones versus the antibiotics cannot explain the correlation observed for SiO₂-GOQDs modified electrode. Indeed,

enhancement in the electrochemical response of modified electrode was augmented in the next series of analytes: SMZ (14%) < TMP (87%) < EST (220%) < DES (760%). This correlation corresponds to the ability of the analytes to form π - π stacking complexes. Particularly, DES is the only compound among investigated, containing two conjugated benzene rings. EST possesses similar molecular geometry but with a single aromatic ring and thus it is less able to form stable π - π stacking complexes. Identically to TMP, SMZ has one aromatic and heterocycle ring, but it has negatively charged sulfamide fragment (Fig S3), which repels from negatively charged GOQDs surface (Fig. 9). Thus, the detection of SMZ was least sensitive among the four substances.

Conclusions

The results demonstrate a great potential of GOQDs for application in electrochemistry. In contrast to GO, nanoparticles of GOQDs can infiltrate in the porous system of the support and thus maintain high surface area of the electrode. CPE modified with SiO₂-GOQDs demonstrated enhanced sensitivity towards DES and EST and less effective towards TMP and SMZ. This fact was explained by significant π - π stacking interaction between immobilized GOQDs and selected hormones. Oxidation peaks for all analytes were shifted to lower potentials for about 100 – 150 mV, demonstrating better interaction between the analytes and active centers of the electrode.

Acknowledgments

Volodymyr Zaitsev is grateful for the financial support received from Conselho Nacional de Desenvolvimento Científico e Tecnológico (CNPq) (grants 306992/2018-3 and 438450/2018-3) and Fundação Carlos Chagas Filho de Amparo à Pesquisa do Estado do Rio de Janeiro (FAPERJ) (grants E-26/010.000978/2019, E-26/210.547/2019). Mikhrallieva is grateful to CNPq (154820/2015-6) and (FAPERJ) (E-26/200.612/2018) for the conceded fellowships. Nazarkovsky thanks to Coordenação de Aperfeiçoamento de Pessoal de Nível Superior (CAPES) for receiving funds (grant № 2013037-31005012005P5 – PNPd-PUC Rio) to carry out the research. We also appreciate the technical support received from Brazilian Nanotechnology National Laboratory (LNNano) in XPS and Institute of Chemistry at UFRGS in CP/MAS 13C NMR. Authors thank LabNano (Brazilian Center for Research in Physics, CBPF, Brazil) for continued assistance in the microscopy studies. Also, we thank Dr. Omar Pandoli (PUC-Rio) for Raman measurements.

Conflict of interests

The authors declare that they have no conflict of interest.

Reference

1. Wu X, Hu J, Qi J, et al (2020) Graphene-supported ordered mesoporous composites used for environmental remediation: A review. *Sep Purif Technol* 239:116511. <https://doi.org/10.1016/j.seppur.2020.116511>
2. Ahmad SZN, Wan Salleh WN, Ismail AF, et al (2020) Adsorptive removal of heavy metal ions using graphene-based nanomaterials: Toxicity, roles of functional groups and mechanisms. *Chemosphere* 248:126008. <https://doi.org/10.1016/j.chemosphere.2020.126008>
3. Stoller MD, Park S, Zhu Y, et al (2008) Graphene-Based Ultracapacitors. *Nano Lett* 8:3498–3502. <https://doi.org/10.1021/nl802558y>
4. Wu Q, Chen L, Gao J, et al (2019) Graphene quantum dots-functionalized C18 hydrophobic/hydrophilic stationary phase for high performance liquid chromatography. *Talanta* 194:105–113. <https://doi.org/10.1016/j.talanta.2018.10.005>
5. Sitko R, Zawisza B, Malicka E (2013) Graphene as a new sorbent in analytical chemistry. *TrAC Trends Anal Chem* 51:33–43. <https://doi.org/10.1016/j.trac.2013.05.011>
6. Nodeh HR, Wan Ibrahim WA, Kamboh MA, Sanagi MM (2015) Dispersive graphene-based silica coated magnetic nanoparticles as a new adsorbent for preconcentration of chlorinated pesticides from environmental water. *RSC Adv* 5:76424–76434. <https://doi.org/10.1039/C5RA13450A>
7. Shi R, Yan L, Xu T, et al (2015) Graphene oxide bound silica for solid-phase extraction of 14 polycyclic aromatic hydrocarbons in mainstream cigarette smoke. *J Chromatogr A* 1375:1–7. <https://doi.org/10.1016/j.chroma.2014.11.057>
8. Wang J, Chen Z, Li Z, Yang Y (2016) Magnetic nanoparticles based dispersive micro-solid-phase extraction as a novel technique for the determination of estrogens in pork samples. *Food Chem* 204:135–140. <https://doi.org/10.1016/j.foodchem.2016.02.016>
9. Mehrzad-Samarin M, Faridbod F, Ganjali MR (2019) A luminescence nanosensor for Ornidazole detection using graphene quantum dots entrapped in silica molecular imprinted polymer. *Spectrochim Acta Part A Mol Biomol Spectrosc* 206:430–436. <https://doi.org/10.1016/j.saa.2018.08.026>
10. Liu Q, Shi J, Sun J, et al (2011) Graphene and Graphene Oxide Sheets Supported on Silica as Versatile and High-Performance Adsorbents for Solid-Phase Extraction. *Angew Chemie Int Ed* 50:5913–5917. <https://doi.org/10.1002/anie.201007138>
11. Huang K-J, Liu Y-J, Li J, et al (2014) Ultra-trace determination of polycyclic aromatic hydrocarbons using solid-phase extraction coupled with HPLC based on graphene-functionalized silica gel

- composites. *Anal Methods* 6:194–201. <https://doi.org/10.1039/C3AY41588K>
12. Mahpishanian S, Sereshti H, Ahmadvand M (2017) A nanocomposite consisting of silica-coated magnetite and phenyl-functionalized graphene oxide for extraction of polycyclic aromatic hydrocarbon from aqueous matrices. *J Environ Sci* 55:164–173. <https://doi.org/10.1016/j.jes.2016.02.023>
 13. Santoso E, Ediati R, Kusumawati Y, et al (2020) Review on recent advances of carbon based adsorbent for methylene blue removal from waste water. *Mater Today Chem* 16:100233. <https://doi.org/10.1016/j.mtchem.2019.100233>
 14. Sitko R, Zawisza B, Talik E, et al (2014) Spherical silica particles decorated with graphene oxide nanosheets as a new sorbent in inorganic trace analysis. *Anal Chim Acta* 834:22–29. <https://doi.org/10.1016/j.aca.2014.05.014>
 15. Li M, Tang S, Zhao Z, et al (2020) A novel nanocomposite based silica gel/graphene oxide for the selective separation and recovery of palladium from a spent industrial catalyst. *Chem Eng J* 386:123947. <https://doi.org/10.1016/j.cej.2019.123947>
 16. Czepa W, Pakulski D, Witomska S, et al (2020) Graphene oxide-mesoporous SiO₂ hybrid composite for fast and efficient removal of organic cationic contaminants. *Carbon N Y* 158:193–201. <https://doi.org/10.1016/j.carbon.2019.11.091>
 17. Chen L, Liang J (2020) An overview of functional nanoparticles as novel emerging antiviral therapeutic agents. *Mater Sci Eng C* 112:110924. <https://doi.org/https://doi.org/10.1016/j.msec.2020.110924>
 18. Pan D, Zhang J, Li Z, Wu M (2010) Hydrothermal route for cutting graphene sheets into blue-luminescent graphene quantum dots. *Adv Mater* 22:734–738. <https://doi.org/10.1002/adma.200902825>
 19. Kang S, Kim KM, Jung K, et al (2019) Graphene Oxide Quantum Dots Derived from Coal for Bioimaging: Facile and Green Approach. *Sci Rep* 9:4101. <https://doi.org/10.1038/s41598-018-37479-6>
 20. Liu Y, Wang R, Lang J, Yan X (2015) Insight into the formation mechanism of graphene quantum dots and the size effect on their electrochemical behaviors. *Phys Chem Chem Phys* 17:14028–14035. <https://doi.org/10.1039/c5cp00646e>
 21. Alvand M, Shemirani F (2017) A Fe₃O₄@SiO₂@graphene quantum dot core-shell structured nanomaterial as a fluorescent probe and for magnetic removal of mercury(II) ion. *Microchim Acta* 184:1621–1629. <https://doi.org/10.1007/s00604-017-2134-2>

22. Sun R, Wang Y, Ni Y, Kokot S (2014) Graphene quantum dots and the resonance light scattering technique for trace analysis of phenol in different water samples. *Talanta* 125:341–346. <https://doi.org/10.1016/j.talanta.2014.03.007>
23. Wu Q, Sun Y, Gao J, et al (2018) Ionic liquid-functionalized graphene quantum dot-bonded silica as multi-mode HPLC stationary phase with enhanced selectivity for acid compounds. *New J Chem* 42:8672–8680. <https://doi.org/10.1039/C7NJ05200F>
24. Choi S-H (2017) Unique properties of graphene quantum dots and their applications in photonic/electronic devices. *J Phys D Appl Phys* 50:103002. <https://doi.org/10.1088/1361-6463/aa5244>
25. Gao Y, Zhong S, Xu L, et al (2019) Mesoporous silica nanoparticles capped with graphene quantum dots as multifunctional drug carriers for photo-thermal and redox-responsive release. *Microporous Mesoporous Mater* 278:130–137. <https://doi.org/10.1016/j.micromeso.2018.11.030>
26. Lu L, Zhou L, Chen J, et al (2018) Nanochannel-Confined Graphene Quantum Dots for Ultrasensitive Electrochemical Analysis of Complex Samples. *ACS Nano* 12:12673–12681. <https://doi.org/10.1021/acsnano.8b07564>
27. Shrivastava S, Jadon N, Jain R (2016) Next-generation polymer nanocomposite-based electrochemical sensors and biosensors: A review. *TrAC Trends Anal Chem* 82:55–67. <https://doi.org/10.1016/j.trac.2016.04.005>
28. Mierzwa M, Lamouroux E, Walcarius A, Etienne M (2018) Porous and Transparent Metal-oxide Electrodes: Preparation Methods and Electroanalytical Application Prospects. *Electroanalysis* 30:1241–1258. <https://doi.org/10.1002/elan.201800020>
29. Ozcelikay G, Karadurmus L, Kaya SI, et al (2020) A Review: New Trends in Electrode Systems for Sensitive Drug and Biomolecule Analysis. *Crit Rev Anal Chem* 50:212–225. <https://doi.org/10.1080/10408347.2019.1615406>
30. Chiorcea-Paquim A-M, Enache TA, Oliveira-Brett AM (2018) Electrochemistry of Alzheimer Disease Amyloid Beta Peptides. *Curr Med Chem* 25:4066–4083. <https://doi.org/10.2174/0929867325666180214112536>
31. Tkachenko A, Onizhuk M, Tkachenko O, et al (2019) An Electrochemical Sensor Based On Graphite Electrode Modified With Silica Containing 1-N-Propyl-3-Methylimidazolium Species For Determination Of Ascorbic Acid. *Methods Objects Chem Anal* Vol. 14, N:5–14. <https://doi.org/10.17721/moca.2019.5-14>
32. Rana A, Baig N, Saleh TA (2019) Electrochemically pretreated carbon electrodes and their electroanalytical applications – A review. *J Electroanal Chem* 833:313–332.

<https://doi.org/10.1016/j.jelechem.2018.12.019>

33. Bibi S, Zaman MI, Niaz A, et al (2019) Voltammetric determination of nitrite by using a multiwalled carbon nanotube paste electrode modified with chitosan-functionalized silver nanoparticles. *Microchim Acta* 186:595. <https://doi.org/10.1007/s00604-019-3699-8>
34. Younus AR, Iqbal J, Muhammad N, et al (2019) Nonenzymatic amperometric dopamine sensor based on a carbon ceramic electrode of type SiO₂/C modified with Co₃O₄ nanoparticles. *Microchim Acta* 186:471. <https://doi.org/10.1007/s00604-019-3605-4>
35. Xuan X, Park JY (2018) A miniaturized and flexible cadmium and lead ion detection sensor based on micro-patterned reduced graphene oxide/carbon nanotube/bismuth composite electrodes. *Sensors Actuators B Chem* 255:1220–1227. <https://doi.org/10.1016/j.snb.2017.08.046>
36. Li S, Huang K, Fan Q, et al (2019) Highly sensitive solution-gated graphene transistors for label-free DNA detection. *Biosens Bioelectron* 136:91–96. <https://doi.org/10.1016/j.bios.2019.04.034>
37. El-Shafai NM, Abdelfatah MM, El-Khouly ME, et al (2020) Magnetite nano-spherical quantum dots decorated graphene oxide nano sheet (GO@Fe₃O₄): Electrochemical properties and applications for removal heavy metals, pesticide and solar cell. *Appl Surf Sci* 506:144896. <https://doi.org/10.1016/j.apsusc.2019.144896>
38. de Souza L V., da Rosa DS, Tkachenko OS, et al (2019) The role silica pore structure plays in the performance of modified carbon paste electrodes. *Ionics (Kiel)* 25:3259–3268. <https://doi.org/10.1007/s11581-019-02882-0>
39. Xie X, Sun D, Liu G, Zeng Q (2014) Sensitive and rapid determination of diethylstilbestrol using mesoporous SBA-15 modified electrode. *Anal Methods* 6:1640. <https://doi.org/10.1039/c3ay41977k>
40. Yu C, Ji W, Wang Y, et al (2013) Graphene oxide-modified electrodes for sensitive determination of diethylstilbestrol. *Nanotechnology* 24:115502. <https://doi.org/10.1088/0957-4484/24/11/115502>
41. Ozcelikay G, Karadurmus L, Kaya SI, et al (2019) A Review: New Trends in Electrode Systems for Sensitive Drug and Biomolecule Analysis. *Crit Rev Anal Chem* 50:212–225. <https://doi.org/10.1080/10408347.2019.1615406>
42. Vinoth V, Natarajan LN, Mangalaraja RV, et al (2019) Simultaneous electrochemical determination of dopamine and epinephrine using gold nanocrystals capped with graphene quantum dots in a silica network. *Microchim Acta* 186:681. <https://doi.org/10.1007/s00604-019-3779-9>
43. Zhao Y, Yuan F, Quan X, et al (2015) An electrochemical sensor for selective determination of sulfamethoxazole in surface water using a molecularly imprinted polymer modified BDD electrode. *Anal Methods* 7:2693–2698. <https://doi.org/10.1039/C4AY03055A>

44. Corsini E, Ruffo F, Racchi M (2018) Steroid hormones, endocrine disrupting compounds and immunotoxicology. *Curr Opin Toxicol* 10:69–73. <https://doi.org/10.1016/j.cotox.2018.01.006>
45. Houston TJ, Ghosh R (2020) Untangling the association between environmental endocrine disruptive chemicals and the etiology of male genitourinary cancers. *Biochem Pharmacol* 172:.. <https://doi.org/10.1016/j.bcp.2019.113743>
46. Gonzalez TL, Rae JM, Colacino JA (2019) Implication of environmental estrogens on breast cancer treatment and progression. *Toxicology* 421:41–48. <https://doi.org/10.1016/j.tox.2019.03.014>
47. Azzouz A, Kailasa SK, Kumar P, et al (2019) Advances in functional nanomaterial-based electrochemical techniques for screening of endocrine disrupting chemicals in various sample matrices. *TrAC Trends Anal Chem* 113:256–279. <https://doi.org/10.1016/j.trac.2019.02.017>
48. Lin Z, Huang H, Cheng L, et al (2020) Atomically Dispersed Mn within Carbon Frameworks as High-Performance Oxygen Reduction Electrocatalysts for Zinc–Air Battery. *ACS Sustain Chem Eng* 8:427–434. <https://doi.org/10.1021/acssuschemeng.9b05713>
49. Behera N, Mantry SP, Mohapatra BD, et al (2019) Functional molecule guided evolution of MnO x nanostructure patterns on N-graphene and their oxygen reduction activity. *RSC Adv* 9:27945–27952. <https://doi.org/10.1039/C9RA04677A>
50. Wu K, Zhao Q, Chen L, et al (2019) Effect of Transition-Metal Ion Doping on Electrocatalytic Activities of graphene/polyaniline-M 2+ (Mn 2+ , Co 2+ , Ni 2+, and Cu 2+) Composite Materials as Pt-Free Counter Electrode in Dye-Sensitized Solar Cells. *Polym Technol Mater* 58:40–46. <https://doi.org/10.1080/03602559.2018.1455864>
51. Porada R, Fendrych K, Baś B (2020) The Mn-zeolite/Graphite Modified Glassy Carbon Electrode: Fabrication, Characterization and Analytical Applications. *Electroanalysis*. <https://doi.org/10.1002/elan.201900744>
52. Zhu Y, Wang G, Jiang H, et al (2015) One-step ultrasonic synthesis of graphene quantum dots with high quantum yield and their application in sensing alkaline phosphatase. *Chem Commun* 51:948–951. <https://doi.org/10.1039/c4cc07449a>
53. Gu Q, Ng TCA, Zain I, et al (2020) Chemical-grafting of graphene oxide quantum dots (GOQDs) onto ceramic microfiltration membranes for enhanced water permeability and anti-organic fouling potential. *Appl Surf Sci* 502:144128. <https://doi.org/10.1016/j.apsusc.2019.144128>
54. Mikhralieva A, Zaitsev V, Xing Y, et al (2020) Excitation-Independent Blue-Emitting Carbon Dots from Mesoporous Aminosilica Nanoreactor for Bioanalytical Application. *ACS Appl Nano Mater* 0:acsanm.0c00363. <https://doi.org/10.1021/acsanm.0c00363>

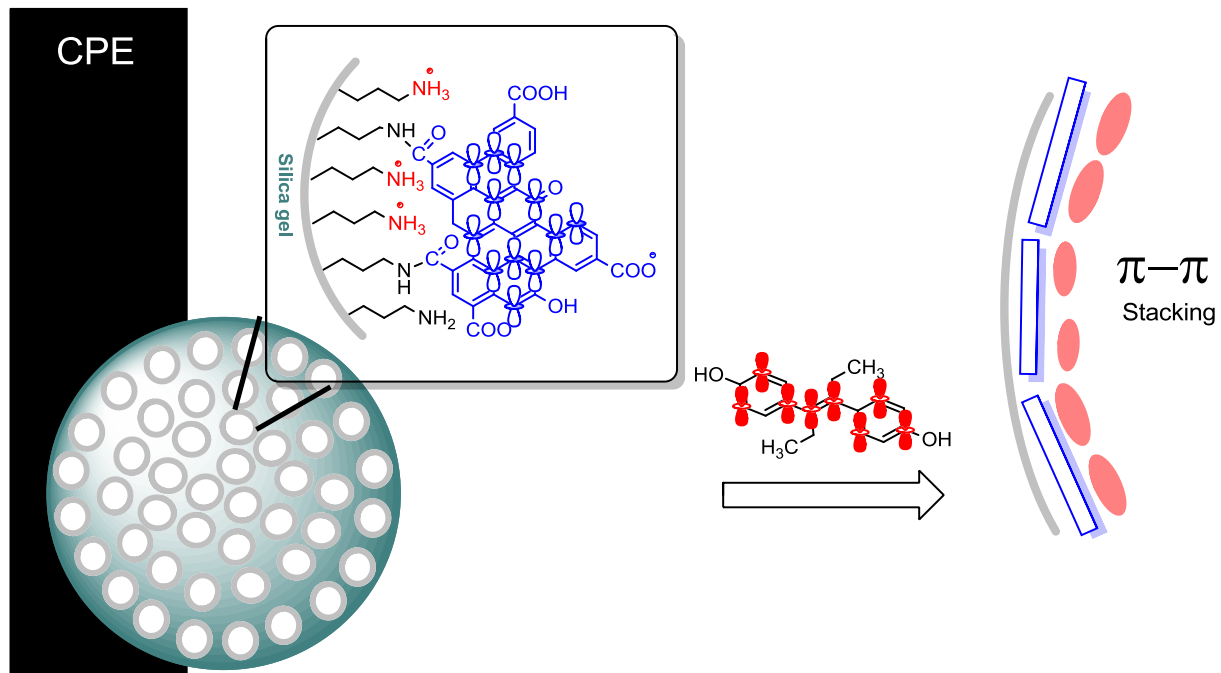
55. Wahab MA, Joseph J, Atanda L, et al (2020) Nanoconfined Synthesis of Nitrogen-Rich Metal-Free Mesoporous Carbon Nitride Electrocatalyst for the Oxygen Evolution Reaction. *ACS Appl Energy Mater* 3:1439–1447. <https://doi.org/10.1021/acsaem.9b01876>
56. Mikhraliieva A, Zaitsev V, Aucélio RQ, et al (2020) Benefit of porous silica nanoreactor in preparation of fluorescence carbon dots from citric acid. *Nano Express* 1:010011. <https://doi.org/10.1088/2632-959X/ab7e0d>
57. Lei He LH, Zhenhong Jia ZJ, and Jun Zhou and JZ (2016) Properties of fluorescence based on the immobilization of graphene oxide quantum dots in nanostructured porous silicon films. *Chinese Opt Lett* 14:041601–041604. <https://doi.org/10.3788/COL201614.041601>
58. Shamaila S, Sajjad AKL, Iqbal A (2016) Modifications in development of graphene oxide synthetic routes. *Chem Eng J* 294:458–477. <https://doi.org/10.1016/j.cej.2016.02.109>
59. Risplendi F, Re Fiorentin M, Cicero G (2020) Unravelling electrocatalytic properties of metal porphyrin-like complexes hosted in graphene matrices. *2D Mater* 7:025017. <https://doi.org/10.1088/2053-1583/ab6a5f>
60. Fernandes DM, Mathumba P, Fernandes AJS, et al (2019) Towards efficient oxygen reduction reaction electrocatalysts through graphene doping. *Electrochim Acta* 319:72–81. <https://doi.org/10.1016/j.electacta.2019.06.175>
61. Chaabane L, Beyou E, El Ghali A, Baouab MH V. (2020) Comparative studies on the adsorption of metal ions from aqueous solutions using various functionalized graphene oxide sheets as supported adsorbents. *J Hazard Mater* 389:121839. <https://doi.org/10.1016/j.jhazmat.2019.121839>
62. Baruah U, Chowdhury D (2016) Ethylene diamine mediated cobalt nanoparticle studded graphene oxide quantum dots with tunable photoluminescence properties. *RSC Adv* 6:67102–67112. <https://doi.org/10.1039/C6RA12686C>
63. Wang L, Wang Y, Xu T, et al (2014) Gram-scale synthesis of single-crystalline graphene quantum dots with superior optical properties. *Nat Commun* 5:5357. <https://doi.org/10.1038/ncomms6357>
64. Gómez-Urbano JL, Gómez-Cámer JL, Botas C, et al (2018) Hydrothermally reduced graphene oxide for the effective wrapping of sulfur particles showing long term stability as electrodes for Li-S batteries. *Carbon N Y*. <https://doi.org/10.1016/j.carbon.2018.06.053>
65. Das TK, Banerjee S, Pandey M, et al (2017) Effect of surface functional groups on hydrogen adsorption properties of Pd dispersed reduced graphene oxide. *Int J Hydrogen Energy* 42:8032–8041. <https://doi.org/10.1016/j.ijhydene.2016.12.024>
66. Li Y, Chen H, Voo LY, et al (2012) Synthesis of partially hydrogenated graphene and brominated

- graphene. *J Mater Chem* 22:15021. <https://doi.org/10.1039/c2jm32307a>
67. Jiangying Q, Feng G, Quan Z, et al (2013) Highly atom-economic synthesis of graphene/Mn₃O₄ hybrid composites for electrochemical supercapacitors. *Nanoscale* 5:2999. <https://doi.org/10.1039/c3nr33700f>
 68. Harremoes P (2013) Hormones as growth promoters: the precautionary principle or a political risk assessment? In: Harremoes P (ed) *The Precautionary Principle in the 20th Century: Late Lessons from Early Warnings*. Routledge, pp 161–169
 69. Tang J, Xiang L, Zhao F, et al (2015) Development of an Up-Conversion Homogenous Immunoassay for the Determination of Diethylstilbestrol in Water. *Anal Lett* 48:796–808. <https://doi.org/10.1080/00032719.2014.961605>
 70. Yin K, Yu F, Liu D, et al (2016) Cyanine-based colorimetric and fluorescent probe for the selective detection of diethylstilbestrol in seawater, shrimp and fish samples. *Sensors Actuators B Chem* 223:799–805. <https://doi.org/10.1016/j.snb.2015.10.014>
 71. Yang Y, Chen J, Shi Y-P (2012) Determination of diethylstilbestrol in milk using carbon nanotube-reinforced hollow fiber solid-phase microextraction combined with high-performance liquid chromatography. *Talanta* 97:222–228. <https://doi.org/10.1016/j.talanta.2012.04.021>
 72. Raymundo-Pereira PA, Campos AM, Vicentini FC, et al (2017) Sensitive detection of estriol hormone in creek water using a sensor platform based on carbon black and silver nanoparticles. *Talanta* 174:652–659. <https://doi.org/10.1016/j.talanta.2017.06.058>
 73. Donini CA, da Silva MKL, Simões RP, Cesarino I (2018) Reduced graphene oxide modified with silver nanoparticles for the electrochemical detection of estriol. *J Electroanal Chem* 809:67–73. <https://doi.org/10.1016/j.jelechem.2017.12.054>
 74. Cesarino I, Cincotto FH, Machado SAS (2015) A synergistic combination of reduced graphene oxide and antimony nanoparticles for estriol hormone detection. *Sensors Actuators, B Chem* 210:453–459. <https://doi.org/10.1016/j.snb.2015.01.013>
 75. Lin X, Li Y (2006) A sensitive determination of estrogens with a Pt nano-clusters/multi-walled carbon nanotubes modified glassy carbon electrode. *Biosens Bioelectron* 22:253–259. <https://doi.org/10.1016/j.bios.2006.01.005>
 76. Zhang S, Wu K, Hu S (2002) Voltammetric determination of diethylstilbestrol at carbon paste electrode using cetylpyridine bromide as medium. *Talanta* 58:747–754. [https://doi.org/10.1016/S0039-9140\(02\)00367-3](https://doi.org/10.1016/S0039-9140(02)00367-3)
 77. Bin Q, Wei W, Chi Y, Chen G (2005) Electrochemical behaviors of diethylstilbestrol and its

application in pharmacokinetics. *Anal Biochem* 336:196–201.
<https://doi.org/10.1016/j.ab.2004.09.028>

78. Lu D, Lin S, Wang L, et al (2012) Synthesis of cyclodextrin-reduced graphene oxide hybrid nanosheets for sensitivity enhanced electrochemical determination of diethylstilbestrol. *Electrochim Acta* 85:131–138. <https://doi.org/10.1016/j.electacta.2012.07.071>
79. Chen C, Chen YC, Hong YT, et al (2018) Facile fabrication of ascorbic acid reduced graphene oxide-modified electrodes toward electroanalytical determination of sulfamethoxazole in aqueous environments. *Chem Eng J* 352:188–197. <https://doi.org/10.1016/j.cej.2018.06.110>
80. Sgobbi LF, Razzino CA, Machado SAS (2016) A disposable electrochemical sensor for simultaneous detection of sulfamethoxazole and trimethoprim antibiotics in urine based on multiwalled nanotubes decorated with Prussian blue nanocubes modified screen-printed electrode. *Electrochim Acta*. <https://doi.org/10.1016/j.electacta.2015.11.151>
81. Cesarino I, Cesarino V, Lanza MRV (2013) Carbon nanotubes modified with antimony nanoparticles in a paraffin composite electrode: Simultaneous determination of sulfamethoxazole and trimethoprim. *Sensors Actuators, B Chem*. <https://doi.org/10.1016/j.snb.2013.08.047>

Graphical abstract



Supplementary information

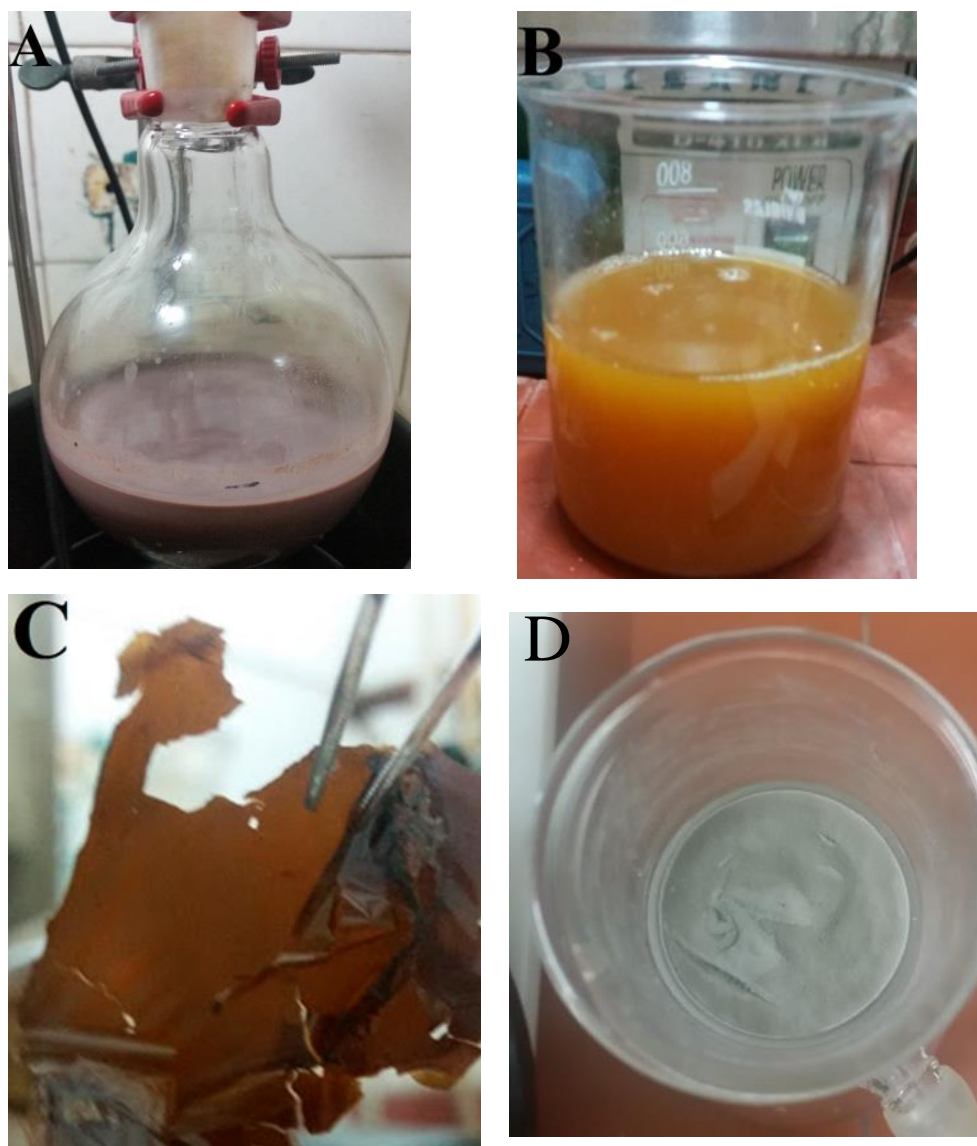


Fig. S1. Digital photos of the reaction mixture after heating during oxidation of graphite (A), after addition of ice and H_2O_2 (B), dry graphene oxide (C) and composite SiO_2 -GOQDs (D)

Table S1 - The results of elemental analysis

Material	N, %	C, %	H, %	C_L^N , mmol/g
SiO_2 - NH_2	1.05	2.89	0.84	0.75
SiO_2 -GOQDs	1.00	3.22	0.86	

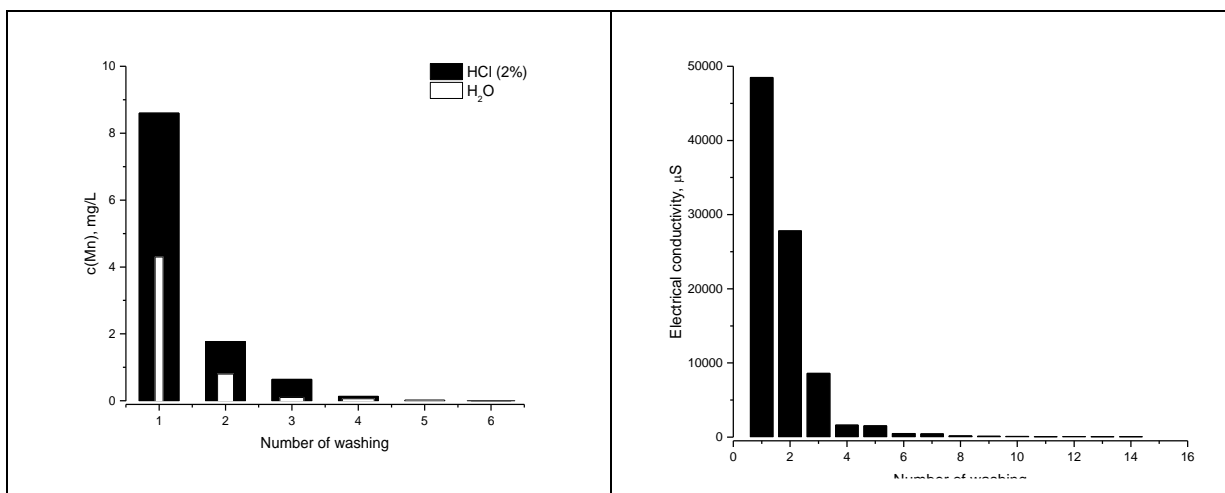


Fig. S2 Effect of washing on $c(\text{Mn})$ in supernatants (a) and monitoring of electrical conductivity with water washing (b)

Table S2 Analytical characteristics of the different electrodes modified with carbogenic nanomaterials in determination of EST, DES, SMZ and TMP

Material	Analyte	Linear range, μmol^{-1}	LOD, μmol^{-1}	LOQ, μmol^{-1}	Equation (y(nA)vsC(μmol^{-1}))	Sensitivity, nA L μmol^{-1}	Ref.
CPE/SiO ₂ -GOQDs	EST	0.01-0.6	0.009	0.029	y=500*C+4.1	500	This work
GCE/CNB/AgNPs		0.2-3	0.16	0.5	n.d.	131	[72]
GCE/rGO/AgNPs		0.1-3	0.021		y=590*C+590	590	[73]
GCE/rGO/SbNPs		0.2-1.4	0.0005		y=2.13*C+0.57	2.13	[74]
GCE/Pt/CNTs		0.5-15	0.62		y=790*C+22040	790	[75]
CPE/SiO ₂ -GOQDs	DES	0.15-0.5	0.18	0.6	y=270*C+32	270	This work
CPE		0.1-15	0.01	0.03	n.d.	n.d.	[76]
CPE/SBA-15		0.0075-0.3	0.003		n.d.	n.d.	[39]
GCE		2-100	0.08		y=337*C+264	337	[77]
GCE/GO/CS		0.015-30	0.003	0.01	y=-69.1*C-1.83	69	[40]
GCE/rGO/CD		0.01-13	0.004		n.d.	n.d.	[78]
CPE/SiO ₂ -GOQDs	SMZ	4-20	0.46	1.53	y=19*C+95.90	19	This work
CPE/MCM-41		98-327	3.1		y=2.43*C+11352	2.43	[38]
CPE/CNTs		1.4-119	0.4	1.33	n.d.	24.1	[32]
SPE/rGO		0.5-50	0.04	0.13	n.d.	n.d.	[79]
MIP/BDD		0.1-100	0.024	0.080	y=314.22*C+7.17	314	[43]
CPE/SiO ₂ -GOQDs	TMP	0.7-3.5	0.191	0.63	y=100*C+106	100	This work
SPE/CNTs/PBnc		0.1-10	0.06	0.2	y=108.31*C+70.7	108	[80]
CPE/CNTs/SbNPs		0.1-0.7	0.031	0.1	y=0.37*C+30	0.37	[81]

Electrodes: CPE – carbon paste electrode; GCE - glassy carbon electrode; MIP - molecularly imprinted polymer; SPE - screen-printed electrode.

Modifiers: CNB – carbon black nanoballs; AgNPs - silver nanoparticles; SbNPs - antimony nanoparticles; AuNPs - gold nanoparticles; rGO - reduced graphene oxide; CoPc - cobalt phthalocyanine; CS - chitosan; CD - β -cyclodextrin; CNTs – carbon nanotubes; BDD - boron-doped diamond; PBnc - Prussian blue nanocubes.

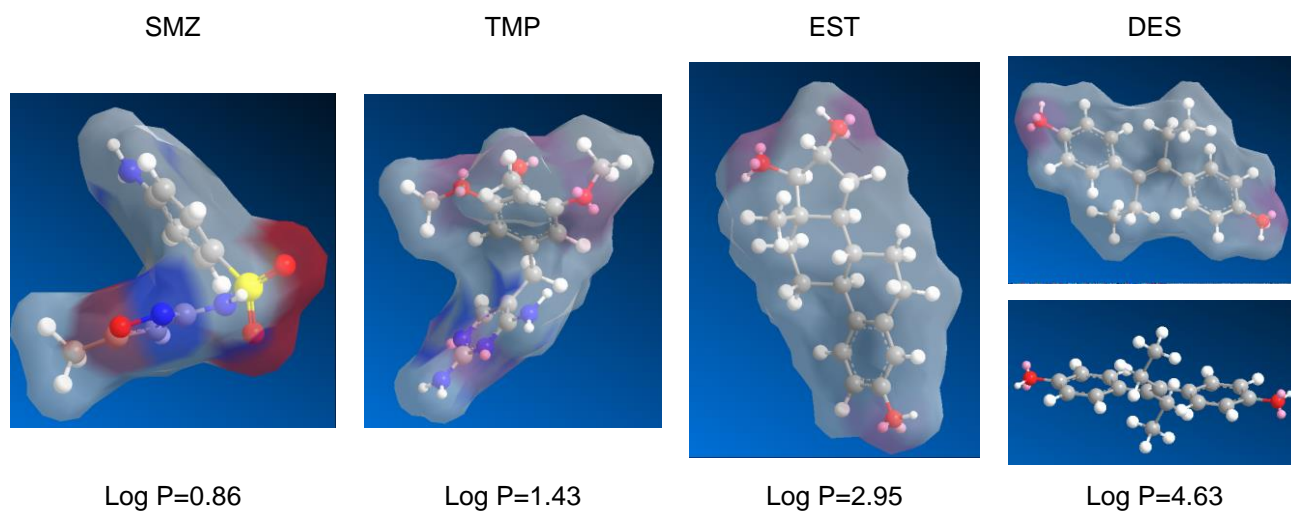


Fig. S 3. Polarity of the selected analytes calculated by software ChemDraw Ultra 12.0